


# Characterizing Positional Sensitivity of Low-Cost Load Cells for IoT-Based Weighing Systems

<sup>1,\*</sup>Curie Habiba, <sup>2</sup>Adhie Prayogo 

<sup>1</sup> Department of Informatics Engineering, Faculty of Engineering, Universitas Muria Kudus, Kudus Regency, Central Java 59327, Indonesia

<sup>2</sup> Department of Industrial Engineering, Faculty of Engineering, Universitas Muria Kudus, Kudus Regency, Central Java 59327, Indonesia

\* Corresponding Author: curie.habiba@umk.ac.id

**Abstract:** Accurate weight measurement is essential for various IoT applications, especially when using low-cost single-point load cells. However, the accuracy is often affected by the load position on the platform. This study investigates the measurement accuracy and stability of a 5 kg single-point load cell with load placement variation. A 30 × 30 cm plywood was mounted over the sensor, with 25 representative load positions were selected. Experiments were conducted using 200 and 500 g weights, each repeated ten times per position. Results show that measurements near the sensor's load application point, the platform's center, had the highest accuracy up to ±99.90%, with RMSE below 1 g, while loads placed near the corners exceeded 2.37 g. Despite variation, the standard deviations remained consistently low, indicating stable sensor behavior. Therefore, a 20 × 20 cm platform is recommended for high accuracy. The results provide valuable insight into platform design and load cell placement, especially for cost-effective and reliable weighing systems in IoT environments.

**Keywords:** IoT, Load Cell Sensors, Weighing System, Positional Accuracy, Calibration.



**Citation:** Habiba, C., & Prayogo, A. (2025). Characterizing positional sensitivity of low-cost load cells for IoT-based weighing systems. *Iota*, 5(3), 2–25.  
<https://doi.org/10.31763/iota.v5i3.1002>

Academic Editor: Adi, P.D.P

Received: June 12, 2025

Accepted: July 16, 2025

Published: August 22, 2025

**Publisher's Note:** ASCEE stays neutral about jurisdictional claims in published maps and institutional affiliations.



**Copyright:** © 2025 by authors. Licensee ASCEE, Indonesia. This article is an open-access article distributed under the terms and conditions of the Creative Commons Attribution-Share Alike (CC BY SA) license(<https://creativecommons.org/licenses/by-sa/4.0/>)

## 1. Introduction

Internet of Things experiences a considerable increase in its influence on the design and deployment of smart systems in Industry, varying from autonomous production, warehouse logistics, smart building, education, product development, IoT-based cloud systems, smart cities, and smart monitoring systems [1]. Concerning the smart monitoring system, several methods may support the concepts, including the RFID [2]–[7], computer vision [8]–[12], or weighing system [13]–[15], which have high potential for real-time monitoring, automation, and data visibility [16]. To be detailed, the weighing system utilizes a load cell, a transducer that converts the applied force into an electric signal, for presenting reliable and accurate weight measurements that can be integrated into IoT infrastructure. To provide high accuracy and reliability in performance, an industrial-grade load cell could be the alternative[17]. However, its complexity and cost do not match the application of IoT in a cost-sensitive and low-scale level. Therefore, the implementation of low-cost single-point load cells arises as a beneficial alternative for small to medium-sized businesses to implement IoT [18].

Although offering accessibility and affordability benefits, a low-cost load cell often faces challenges, such as stability and accuracy, especially while running outside of its ideal configuration [19]. One critical yet often overlooked factor that may influence the performance is the load position on the weighing platform. In an ideal scenario, the load is mounted exactly on the load application point, which is usually the center above the strain gauge. However, in real-world applications, objects may be placed off the center, or even randomly, which may result in inconsistent and erroneous readings [20]. In relation to the complexity, a single point load cell is designed with different platform size standards, which, unfortunately, is not documented properly. As a result, there are variations in design assumption, which has a vital role in load distribution and sensor response.

This study aims to evaluate the reading performance of a low-cost and unbranded single-point load cell installed under a 30 cm x 30 cm plywood platform. The size is chosen as it is commonly recommended for low-cost load cells in the market. Also, the size covers the upper limit of the recommended range, making it more relevant for the sensor's performance evaluation under real conditions. The focus of this study is to systematically investigate how load position variations across the plywood platform affect the stability and accuracy of the load cell readings. A moving average method for filtering noisy ADC readings and a two-point linear equation method for calibration against known reference weights are deployed to ensure reliability. Furthermore, by highlighting both the potential and limitations of using low-cost single-point load cells under non-ideal loading positions, the research attempts to enrich practical insights for academicians, IoT practitioners, and developers who aim to implement a weighing mechanism in their systems.

## 2. Theory

### 2.1 Weight Measurement and Load Cells

Low-cost weight sensors, typically based on single-point load cells coupled with ADC modules, offer affordability and simplicity. The system has become widely adopted for IoT applications [21]. A load cell usually operates on the principle of strain gauges, where the applied load deforms the sensor and then changes the electrical resistance of the strain gauge. The electrical resistance changes are then converted into a proportional voltage or digital signal using an analog-to-digital converter (ADC) module such as the HX711[22].

### 2.2 Sources of Error in Load Cell Measurement

During the applications, the load cell readings are rarely free from error[23], [24]. Offset and drift are commonly found error sources that occur when the sensor produces a nonzero output when there is no applied load on the platform, or when the reading value slowly changes over time, even though there are no changes in applied load, because of temperature variations or electronic instability. In addition, the sensor performance may be affected by whether the load is applied or removed, even if the weight is the same, which is called hysteresis [25]. That phenomenon is commonly caused by mechanical stress and the material properties of the load cell.

Another important factor that causes errors is the load position on the weighing platform. Ideally, the sensor should generate consistent readings regardless of placement. However, in practice, the output may differ when the weight is placed at different positions over the weighing platform, particularly near the edges or corners. This effect is influenced by several causes, including sensor mounting, platform rigidity, and the quality of force transfer from the platform to the sensor. These error sources emphasize the need for careful calibration, stable platform design, and proper data processing strategies to achieve accurate and reliable weight measurements.

Several manufacturers of single-point load cells usually provide recommendations for the platform's maximum size, as shown in Table 1. The recommendations assist the user in having more reliable readings by minimizing errors due to uneven load distribution and mechanical stress on the sensor. Unfortunately, many low-cost load cells in the market were not equipped with such specification recommendations or clear guidelines for proper assembly and platform integration. Previous studies have examined the effect of load placement on sensor readings, presenting the influence of object position on measurement performance. However, these studies often focus on overall deviations without presenting the spatial distribution of errors across the platform and its explanation.

**Table 1.** Maximum Recommendations

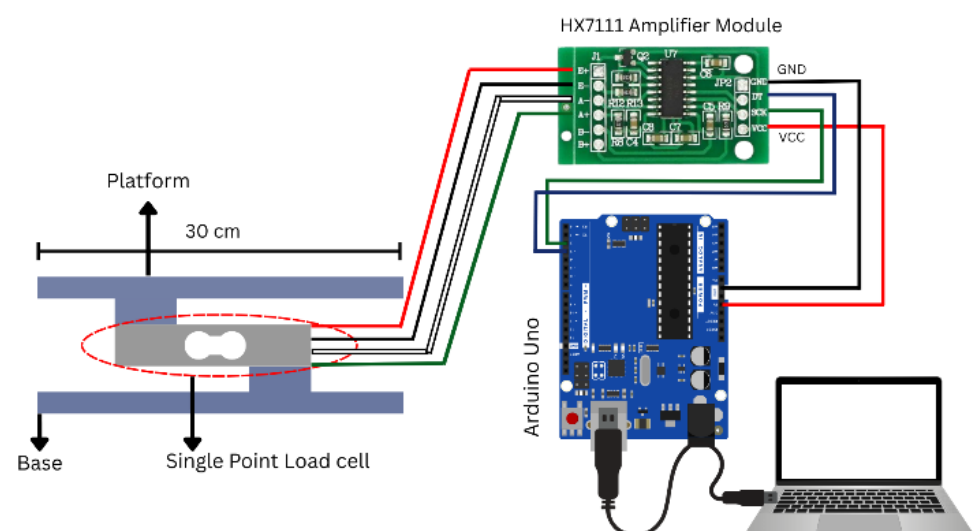
Brand	Type	Off-center load compensation
SCAIME [26]	FT-BEF-F-FE-0921	15 × 15 cm
VALCOM [27]	VPW6DC3	30 × 30 cm
Minebea intec [28]	BCL-A	30 × 30 cm
ANYLOAD [29]	108AA	23 × 23 cm
HBK [30]	Single Point Load cell PW4M	20 × 20 cm
Cardinal [31]	TSP LoadCells	40 × 40 cm

### 3. Method

#### 3.1 System Design and Hardware Configuration

This study designed and deployed a low-cost weighing system to present realistic constraints in IoT-based applications. Easily accessible and affordable materials were chosen for the system assembly to allow replicability and relevance of low-budget implementations. The built system uses the main hardware components, shown in Table 2, as follows:

- A single point load cell with a rated capacity of 5. It is an unbranded, affordable type and widely available in online marketplaces.
- A plywood platform with a defined size of 30 cm × 30 cm, considering the upper limit of the recommended size range (10–30 cm), which is common for this class of load cells.
- A sensor holder that was printed by 3D printing. It was designed to protect the load cell installed on a rigid base structure and, also, to maintain stable alignment during measurements.
- An analog-to-digital converter (ADC) module specifically used for load cells, called HX711. It is for amplifying the millivolt output signal obtained from the load cell and further interfaces it with the microcontroller.
- An Arduino Uno microcontroller, selected because of its cost-effectiveness, ease of programming, and wide adoption in academic and prototyping concepts.
- A personal laptop, used for data acquisition, visualization, and basic processing.

**Figure 1.** System Architecture

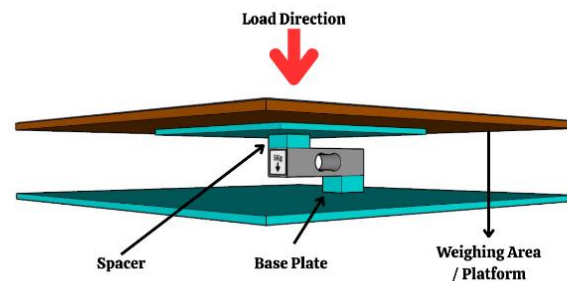


**Figure 2.** System Design

**Table 2.** System Specifications

Item	Specifications
Load cell	Unbranded low-cost load cell sensor with a 5 Kg maximum load
Platform	30 × 30 × 0.7 cm Ply wood
Spacer	Custom 3D Print (PLA)
HX7111	Amplifier Module
Arduino Uno	Microcontroller
Laptop	For the data record and processing unit

Figure 1 and 2 depicts the system architecture and system design, respectively, by assembling all previously mentioned components. In detail, Figure 1 shows the load cell firmly mounted onto the 3D-printed holder, which together then fixed onto a stable base. Figure 2 illustrates how the plywood platform was attached to the load cell, aligned with its load application point.

### 3.2 Load Position Mapping

Furthermore, to determine the load placement on the plywood platform while assessing its effect on stability and accuracy readings, a spatial sampling approach was used. The plywood platform's top surface was divided into an 8 × 8 matrix, forming a total of 64 square-shaped regions. Based on this grid, 25 representative regions were selected for positioning the load, including both central and peripheral areas, to ensure coverage across the platform. Each test point was defined using a Cartesian coordinate system, where the origin (0,0) represents the mechanical center of the platform. The center is vertically aligned with the load application point of the load cell, depicted in Figure 3. In detail, coordinates were expressed in grid units. The x-axis was oriented to the horizontal line while the y-axis to the vertical line, with the perspective of the observer facing the platform from above, depicted in Figure 4. Each grid area was physically marked on the platform surface to assist the user in ensuring consistent load placement during measurement, which further enables a structured analysis of measurement results' stability and accuracy. Figure 5 presents the actual integration of the hardware components of the system for experimental phases.

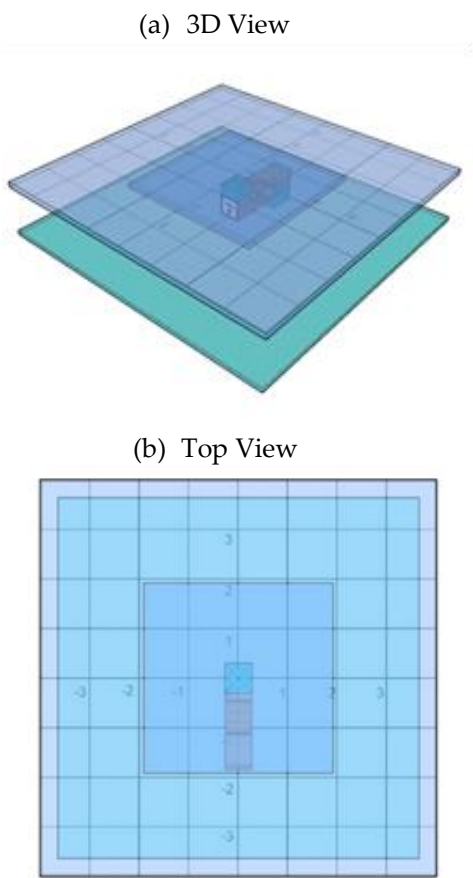


Figure 3. (a, b) Platform Design

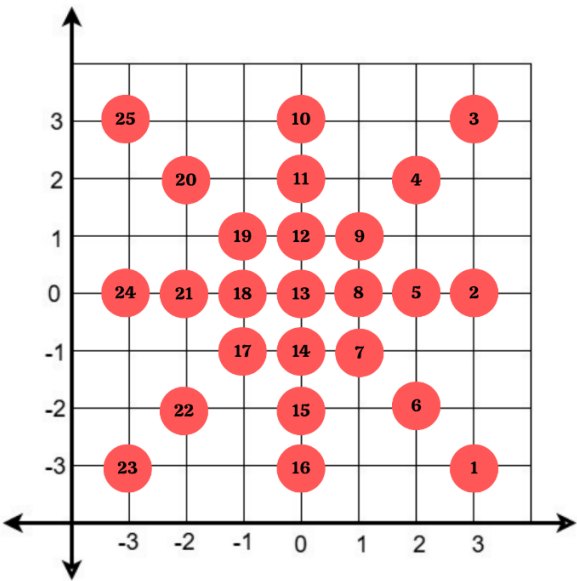
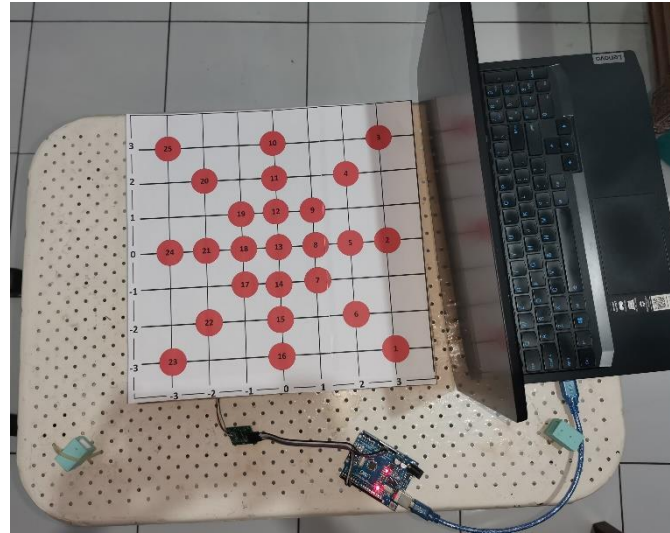


Figure 4. Selected Points on Platform



**Figure 5.** Implementation

### 3.3 Signal Filtering

Fluctuations in sensor readings are commonly found in low-cost weighing systems due to several reasons, including electrical noise, mechanical vibrations, and environmental factors. The applied moving average filter smooths the raw analog-to-digital converter (ADC) readings obtained from the HX711 module, increasing the stability and reliability. The moving average algorithm operates by continuously computing the average of a fixed number of the most recent samples in the signal stream. The filtered signal is  $\bar{x}_i$  at index  $i$  can be expressed mathematically as equation 1.

$$\bar{x}_i = \frac{1}{N} \sum_{j=i-N+1}^i x_j \quad (1)$$

Where:

- $\bar{x}_i$  represents the raw ADC value at sample  $j$ ,
- $N$  is the window size, the number of samples considered in each averaging cycle.

This method attenuates short-term fluctuations and transient spikes effectively, which further provides a more stable signal for downstream processing. In this study, a window size of  $N=10$  was selected empirically, as it provided a good balance between response time and smoothness without introducing excessive lag. Then, the filtered output was used as an input to the calibration function for accurate weight calculation.

### 3.4 Calibration Procedure

Load cells usually possess a linear relationship between the applied load and the analog voltage output generated by the strain gauges. With the assumption of running the system without any mechanical distortion and within its rated range, the digital value obtained from the HX711 module maintains a proportional and linear correlation to the applied load. According to this linearity, a two-point calibration method was used to map the ADC output to actual weight values.

In terms of calibration, the process involved placing two standardized reference weights, including 200 and 500 g, at the center of the platform, position (0,0). For each weight, the corresponding filtered ADC output was recorded. Let  $(x_1, y_1)$  and  $(x_2, y_2)$  represent the ADC values and corresponding known weights for the 200 g and 500 g references, respectively. A linear relationship between the ADC reading and the weight was assumed following the equation of a line, as the Equation 2.

$$\text{Weight} = m \cdot \text{ADC} + b \quad (2)$$

The slope  $m$  and intercept  $b$  were determined using the standard two-point formula as equation 3.

$$m = \frac{y_2 - y_1}{x_2 - x_1}, \quad b = y_1 - m \cdot x_1 \quad (3)$$

### 3.5 Experimental Procedure

In this experiment in investigating the effects of the load placement on reading accuracy and stability, a series of controlled measurements was performed using the already mapped platform, as described in Section 3.B. Two reference weights, including 200 g and 500 g, were selected for this experiment. The platform, 30 cm × 30 cm in size, was divided into an 8 × 8 grid (64 squares in total), and 25 selected positions, shown in Figure 5, were mapped into coordinate points with the center around the load application point (0, 0). The full list of sample point coordinates is detailed in Table 3.

**Table 3.** List of Coordinates

Position ID	Coordinate (x, y)
1	(3, -3)
2	(3, 0)
3	(3, 3)
4	(2, 2)
5	(2, 0)
6	(2, -2)
7	(1, -1)
8	(1, 0)
9	(1, 1)
10	(0, 3)
11	(0, 2)
12	(0, 1)
13	(0, 0) ( <i>center</i> )
14	(0, -1)
15	(0, -2)
16	(0, -3)
17	(-1, -1)
18	(-1, 0)
19	(-1, 1)

Position ID	Coordinate (x, y)
20	(-2, 2)
21	(-2, 0)
22	(-2, -2)
23	(-3, -3)
24	(-3, 0)
25	(-3, 3)

At each coordinate point on the map, both the 200 g and 500 g weights were placed individually. For each placement:

- The ADC output was filtered using a moving average as described in Section 3.C.
- The filtered ADC value was converted into weight using the calibration equation from Section 3.D.
- The measurement was repeated 10 times at each point to observe the output variation and compute the average error to ensure stability and accuracy, respectively.

This repetition of measurement facilitates a systematic error assessment, especially for the bias that arises from off-center placement, and random variation or instability affected by structural or signal noise. Further, the error could be quantified by comparing the measured weight to the real value, while the stability was measured by calculating the standard deviation across the ten measurements for each position.

To minimize measurement error while doing the experiment, caused by how loads are placed on the platform, a systematic loading procedure is structured as follows:

- Place the load at the center of the designated platform mark to avoid eccentric loading and induced torque
- Apply loads carefully and then wait a fixed settling time (5s approximately) before recording to let the mechanical creep and electronic filtering stabilize.
- For each test point, take multiple readings (10)
- Control environmental factors (isolate the system from unexpected vibration, keep a stable temperature).

#### 4. Result and Analysis

To evaluate the accuracy and consistency of the load cell across various placement positions on the platform, two standard weights (200 g and 500 g) were applied at each of the 25 mapped positions. Each measurement was repeated 10 times to account for variability and to assess measurement stability. The average measured weight, average ADC value, absolute error, and standard deviation at each point were computed using the calibration from equation (2):

$$\text{Weight(g)} = 0.002521 \times \text{ADC} + 0.29$$

To evaluate the accuracy of the weight sensor, the observed measurement errors were quantified using Mean Absolute Error (MAE) and Root Mean Square Error (RMSE). In detail, the MAE measures the average magnitude of the errors without considering their



direction, either positive or negative, making it useful for understanding overall deviation from the real values. It is calculated with equation 4, as follows:

$$MAE = \frac{1}{n} \sum_{i=1}^n |y_i - \hat{y}_i| \quad (4)$$

where  $y_i$  represents the actual (reference) weight,  $\hat{y}_i$  is the measured weight, and  $n$  is the total number of observations. On the other hand, the RMSE gives higher weight to larger errors, making it more sensitive to outliers. It is calculated with equation 5, as follows:

$$RMSE = \sqrt{\frac{1}{n} \sum_{i=1}^n (y_i - \hat{y}_i)^2} \quad (5)$$

Analyzing both MAE and RMSE allows the observer to have a more comprehensive understanding of the sensor's performance, where MAE reflects the typical error magnitude, and RMSE emphasizes the impact of larger deviations. Moreover, to observe the stability of the sensor readings, each measurement point was calculated for its Standard Deviation (Std. Deviation). The standard deviation quantifies the amount of variation or dispersion from the mean value. It is computed using equation 6, as follows:

$$\text{Std. Deviation} = \sqrt{\frac{1}{n} \sum_{i=1}^n (\hat{y}_i - \bar{y})^2} \quad (6)$$

where  $\bar{y}$  is the mean of the readings,  $\hat{y}_i$  is the measured weight. Analyzing the Std. Deviation enables the user to assess the consistency of sensor outputs, in which lower values indicate that the readings are tightly clustered around the mean, reflecting better stability and reduced noise in the measurement process.

To evaluate the accuracy, a comparison between the measured weight obtained from the sensor readings with the actual known weight using the relationship between absolute error and true value was conducted. The overall accuracy for multiple measurements was assessed by using Mean Absolute Percentage Error (MAPE) by equation 7, as follows:

$$MAPE = \frac{1}{n} \sum_{i=1}^n \left| \frac{\hat{y}_i - y_i}{y_i} \right| \times 100\% \quad (7)$$

The percentage accuracy was then determined using:

$$\text{Accuracy (\%)} = 100\% - \text{MAPE} \quad (8)$$

#### 4.1 Results for 200 g Load

A 200 g standard mass was placed systematically across 25 predefined locations on the platform, enabling investigation of the load cell's sensitivity to positional variation. Each position was experimented with for ten repetitions, allowing the calculation of

average weight readings, average ADC values, mean absolute error, associated standard deviation, and the accuracy. Table 4 presents the detailed performance metrics of the light load level, 200 g, for each position, delivering insights into how load placement affects both accuracy and consistency.

**Table 4.** Performance Metrics of 200 g

Pos	Coord	Avg. Weight (g)	Avg. ADC	Mean Abs Error (g)	Accuracy (%)	Std. Deviation (g)
1	(3, -3)	197.69	78191	0.217	99.89	0.024
2	(3, 0)	198.04	78333	0.218	99.89	0.031
3	(3, 3)	198.11	78362	0.037	99.98	0.031
4	(2, 2)	198.83	78670	0.042	99.98	0.043
5	(2, 0)	199.22	78830	0.094	99.95	0.022
6	(2, -2)	198.60	78570	0.061	99.97	0.017
7	(1, -1)	199.36	78891	0.033	99.98	0.024
8	(1, 0)	199.54	78967	0.029	99.99	0.029
9	(1, 1)	199.31	78874	0.022	99.99	0.021
10	(0, 3)	199.43	78922	0.123	99.94	0.024
11	(0, 2)	199.30	78869	0.135	99.93	0.025
12	(0, 1)	199.48	78949	0.115	99.94	0.016
13	(0, 0)	199.68	79029	0.046	99.98	0.008
14	(0, -1)	199.45	78931	0.028	99.99	0.012
15	(0, -2)	198.86	78618	0.032	99.98	0.033
16	(0, -3)	198.25	78330	0.085	99.96	0.082
17	(-1, -1)	198.72	78626	0.102	99.95	0.020
18	(-1, 0)	199.29	78865	0.106	99.95	0.023
19	(-1, 1)	199.50	78956	0.153	99.92	0.029
20	(-2, 2)	199.17	78814	0.388	99.81	0.023
21	(-2, 0)	199.26	78853	0.107	99.95	0.013
22	(-2, -2)	198.47	78490	0.127	99.94	0.046
23	(-3, -3)	198.21	78388	0.154	99.92	0.032
24	(-3, 0)	198.42	78476	0.123	99.94	0.047
25	(-3, 3)	198.68	78600	0.312	99.84	0.029

According to Table 4, a relatively high accuracy ( $\geq 99.9\%$ ) was recorded in the central region of the platform, primarily between coordinates (0, 0) and (1, 1), where the MAE was consistently under 0.2 g. This area coincides with the known load application point, strengthening the idea that the sensor’s optimal precision is near its center.

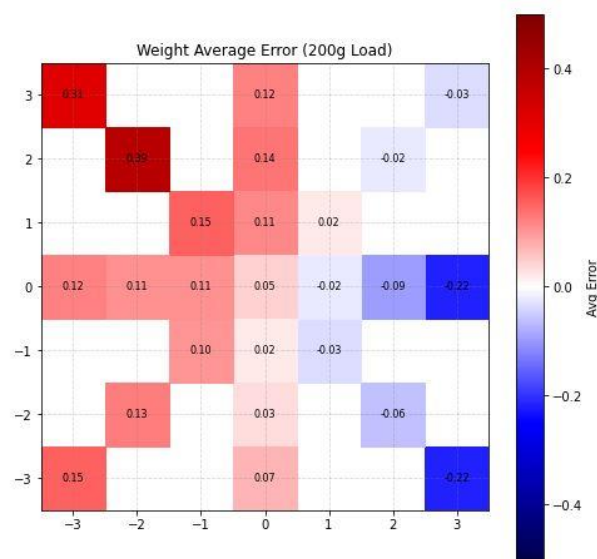


**Figure 6.** Error Distribution (200 g)

On the contrary, an increased value of MAE exceeding 0.3 g and slightly higher standard deviations were observed on the edges and corners. These deviations suggest a sensitivity to load eccentricity, where minor platform tilt or asymmetric deformation likely affected strain distribution and sensor response. However, even at the worst positions, the maximum observed MAE remained under 0.4 g, indicating acceptable performance for many non-critical applications. The distribution of the weight average error is shown in Fig. 6. In the case of standard deviations, the value remained relatively stable ( $<0.1$ ) across all positions, indicating consistent repeatability even when accuracy varied, which is critical for applications that rely on relative rather than absolute measurements.

#### 4.2 Results for 500 g Load

In terms of assessing the effect of higher mass on positional measurement stability, the same experimental procedure was repeated using a 500 g load. This load represents a more substantial mechanical effect on the platform and allows assessment of whether increased force alters the spatial distribution of sensor error or amplifies non-linear mechanical effects. Table 5 presents a summary of the quantitative results of how the sensor's output responds to placement changes of the applied weight.

Table 5. Performance Metrics of 500 g

Pos	Coord	Avg. Weight (g)	Avg. ADC	Mean Abs Error (g)	Accuracy (%)	Std. Deviation (g)
1	(3, -3)	496.59	196591	3.41	99.32	0.047
2	(3, 0)	497.39	197388	2.73	99.45	0.020
3	(3, 3)	497.12	197129	1.78	99.64	0.049
4	(2, 2)	498.03	198028	0.96	99.81	0.041
5	(2, 0)	498.74	198744	1.32	99.74	0.021
6	(2, -2)	497.51	197510	1.69	99.66	0.019
7	(1, -1)	499.11	199106	0.41	99.92	0.011
8	(1, 0)	499.45	199453	0.28	99.94	0.054
9	(1, 1)	499.20	199204	0.38	99.92	0.060
10	(0, 3)	499.33	199330	0.19	99.96	0.014
11	(0, 2)	499.27	199265	0.15	99.97	0.070
12	(0, 1)	499.52	199517	0.04	99.99	0.035
13	(0, 0)	499.90	199900	0.09	99.98	0.044
14	(0, -1)	499.51	199506	0.01	99.99	0.014
15	(0, -2)	498.87	198873	0.11	99.98	0.038
16	(0, -3)	498.02	198017	0.39	99.92	0.020
17	(-1, -1)	498.40	198401	0.20	99.96	0.019
18	(-1, 0)	499.17	199168	0.17	99.97	0.016
19	(-1, 1)	499.42	199420	0.09	99.98	0.023
20	(-2, 2)	498.65	198646	0.19	99.96	0.014
21	(-2, 0)	498.83	198829	0.14	99.97	0.029
22	(-2, -2)	498.14	198137	0.37	99.93	0.022
23	(-3, -3)	496.11	196112	3.87	99.23	0.079
24	(-3, 0)	497.42	197420	2.72	99.46	0.050
25	(-3, 3)	497.80	197802	0.97	99.81	0.046

A similar result to the 200 g measurement was obtained, as the 500 g experiments confirm that the load cell performs best in the central platform area. The MAE were consistently below 0.5 g. This reaffirms that symmetrical loading close to the sensor's central strain axis minimizes error.

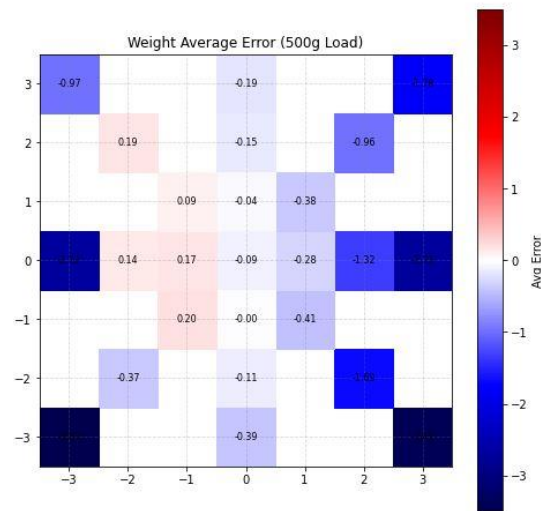


**Figure 7.** Error Distribution 500 g

However, as the force increases, the observed magnitude of peripheral error does grow. To be more detailed, in edge and corner positions, MAE is increased to over 3.87 g, with the highest recorded at (-3, -3). This increased deviation suggests a slight non-linearity in mechanical response or platform flexion under higher mass, despite the calibration itself showing linear ADC behavior. The weighted average error distribution on the platform is shown in Fig. 7.

Standard deviations remained relatively stable ( $<0.1$ ) across all positions, indicating consistent repeatability even when accuracy varied, which is critical for applications that rely on relative rather than absolute measurements.

#### 4.3 Accuracy and Stability by Grid Region

To better interpret the performance of the single-point load cell across different platform zones, the 30 cm  $\times$  30 cm weighing surface was conceptually divided into three radial regions based on proximity to the center:

- First Grid: Includes positions near the center (e.g., (0,0), ( $\pm 1$ , 0), (0,  $\pm 1$ ), ( $\pm 1$ ,  $\pm 1$ )) within approximately 10 -12 cm diameter.
- Second Grid: Intermediate positions, extending approximately 12 - 20 cm from the center.
- Third Grid: Outer and corner regions, beyond 20 cm, covering the periphery of the platform.

Figures 8 and 10 present the results of ten repeated sensor readings at each sampling point across the three grid regions for applied weights of 200 g and 500 g, respectively. These figures illustrate the variation in sensor outputs within each region, where the degree of fluctuation is quantitatively represented by the standard deviation. For both load conditions, the behavior of the standard deviation shows a clear increasing trend from the first region to the third region, indicating that the sensor readings become less stable as the load is positioned farther from the central region. At 200 g, the variation among sampling points remains relatively small across all regions, although a gradual increase in dispersion can still be observed. In contrast, at 500 g, the variation is more pronounced, particularly in the second and third regions, where the differences in

readings between sampling points become significantly larger. This result highlights that the effect of load placement on measurement stability is magnified at higher loads, especially in peripheral regions of the platform.

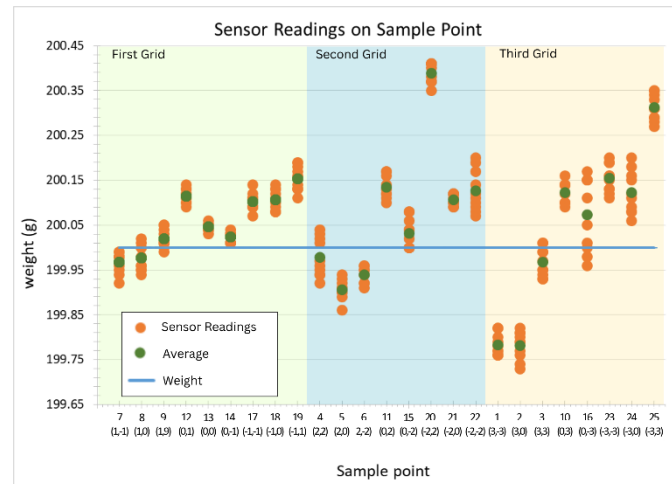


**Figure 8.** Sensor reading on Each Sample Point (200 g)

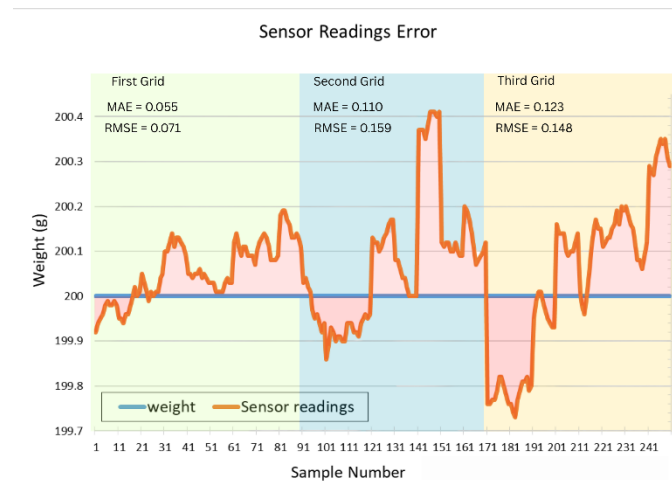


**Figure 9.** Sensor Readings Error (200 g)

Figures 9 and 11 present the distribution of sensor readings across the three grid regions for applied weights of 200 g and 500 g, respectively. In these figures, the horizontal axis represents the sample number, with samples 1–90 corresponding to the first grid region, samples 91–170 to the second grid region, and samples 171–250 to the third grid region. The vertical axis shows the sensor readings expressed in g, which are compared against the reference weights to evaluate the measurement error. The reading errors are quantitatively described using the Mean Absolute Error (MAE) and the Root Mean Square Error (RMSE). The results indicate a pattern in which both MAE and RMSE increase as the measurement location shifts from the first grid to the second grid and further to the third grid. At 200 g, the variation in sensor readings is relatively small, yet a consistent increase in error values is observed from the first to the third grid. At 500 g, this trend becomes more pronounced, with the second and third regions showing a wider spread of readings and, consequently, larger MAE and RMSE values. These findings

demonstrate that the spatial placement of the load strongly affects the accuracy of the sensor, with peripheral regions of the platform yielding higher measurement errors compared to the central region.

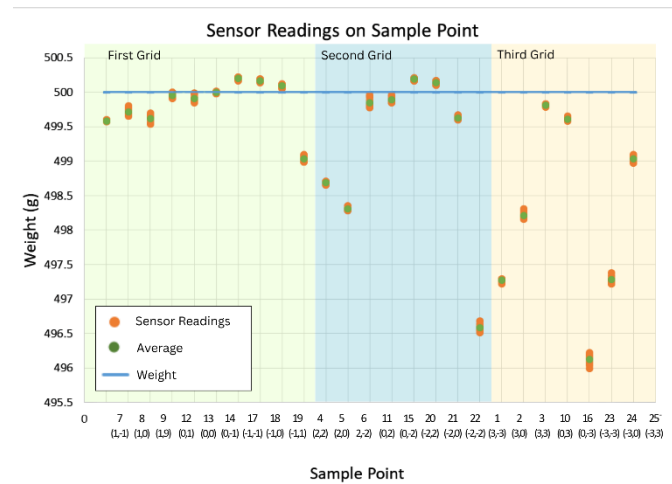


**Figure 10.** Sensor reading on Each Sample Point (500 g)

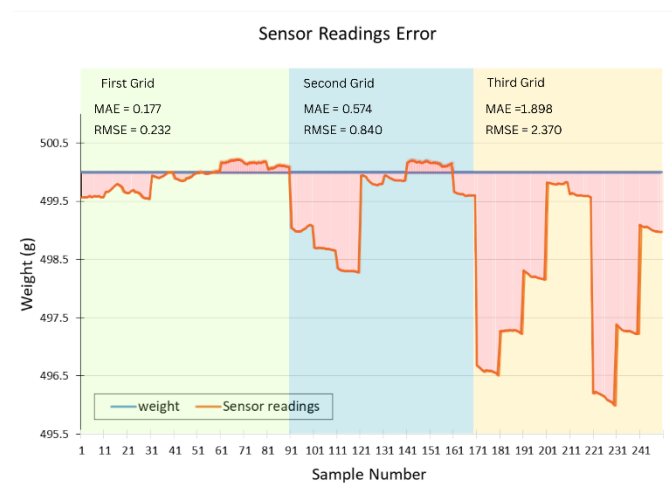


**Figure 11.** Sensor Readings Error (500 g)

The analysis of sensor performance across different grid regions and load conditions demonstrates variations in error metrics and stability. For the first region, the measurement results showed relatively high consistency, with a Mean Absolute Error (MAE) of 0.055 g and Root Mean Square Error (RMSE) of 0.071 g at a 200 g load, yielding an accuracy of 99.97% and a low standard deviation of 0.060 g. At a higher load of 500 g, the MAE and RMSE increased slightly to 0.177 g and 0.232 g, respectively, with an accuracy of 99.96% and a standard deviation of 0.223 g, indicating stable performance.

In the second region, the errors were slightly higher, particularly at the 500 g load, where the MAE and RMSE reached 0.574 g and 0.840 g, respectively, with accuracy decreasing to 99.89% and the standard deviation increasing to 0.703 g. At 200 g, however, the values remained lower, with an MAE of 0.110 g and an accuracy of 99.94%.

The third region exhibited the most notable increase in error at higher load conditions. At 200 g, the MAE was 0.123 g and the RMSE was 0.148 g, with 99.93% accuracy and a standard deviation of 0.158 g, comparable to other regions at the same load. However, when tested with 500 g, the error values increased substantially, with an MAE of 1.898 g, RMSE of 2.370 g, and accuracy dropping to 99.62%, accompanied by a standard deviation of 1.335 g. These findings suggest that while the load cell maintained high accuracy overall, the effect of load placement was more pronounced at higher loads, particularly in the third region, where instability and larger error distributions were observed.

A summary of the average accuracy and stability across the three grid regions is presented in Table 6. This classification provides practical guidance for platform design and sensor placement.

**Table 6.** Average Accuracy and Stability Summary

Region (Grid)	Distance from Center (cm)	Weight (g)	MAE (g)	RMSE (g)	Acc (%)	Std. Dev (g)
First	0 – 10	200	0.055	0.071	99.97	0.060
First	0 – 10	500	0.177	0.232	99.96	0.223
Second	10 – 20	200	0.110	0.159	99.94	0.154
Second	10 – 20	500	0.574	0.840	99.89	0.703
Third	20 – 30	200	0.123	0.148	99.93	0.158
Third	20 – 30	500	1.898	2.370	99.62	1.335

Given these findings, it is recommended to restrict the effective weighing area to a central 20 cm × 20 cm region to ensure reliable results with an accuracy reach  $\pm 99.90\%$ . Alternatively, if full area coverage is desired, the system should be redesigned to include multiple sensors or mechanical structures that can better distribute the applied force across the load cell.

## 5. Conclusions

This study evaluated the performance under varied load positions of a 5 kg single-point load cell on a 30 × 30 cm wooden platform, focusing on accuracy and stability for weights of 200 g and 500 g. The platform was divided into an 8×8 grid, and 25 representative load positions were selected to simulate a broad range of practical loading conditions.

The results showed that the load position and the heavier load significantly influence measurement accuracy, while the stability remained consistently high across all regions. The highest accuracy was observed near the center of the platform, particularly within a 10 cm radius of the load application point, where MAE remained below 1 g and standard deviations below 1 g. As the load was moved further from the center, particularly beyond 20 cm, the MAE increased noticeably, exceeding 1.898 g for the 500 g load.

Despite these variations in positional accuracy, the standard deviation of repeated measurements for each sample point was generally low, specifically below 0.1 g, which indicates reliable and stable performance. This suggests that while raw measurements at peripheral positions may be less accurate, they are still repeatable and could be corrected through an algorithmic compensation or calibration.



Based on these findings, it is recommended that:

- For applications requiring high accuracy, such as digital weighing or inventory control, the effective platform area using a single point load cell is limited to 20 × 20 cm when the platform is mounted at the center of the platform.
- For wider platform utilization, additional load cells or mechanical redistribution structures should be considered to improve force coupling with the sensor.
- Calibration strategy or correction matrices may be implemented to extend usable platform space while maintaining acceptable measurement accuracy.

These insights are particularly relevant for designing low-cost, IoT-based weighing systems where spatial accuracy is a critical consideration in the choice and implementation of load cells.

## 6. Future Research

For future research, the study will focus on enhancing the weighing platform by developing a more rigid and durable structure, enabling the system to handle and test higher loads and a wider platform with improved accuracy. Additionally, a weighing system will be constructed using four load cells integrated into a single platform, allowing for a more uniform distribution of weight measurement across the platform. This configuration will be used to observe and analyse the effects of load position on measurement accuracy, providing deeper insights into load distribution and sensor behaviour for different weighing system designs. Beyond the mechanical and sensor aspects, the research will also explore the Quality of Service (QoS) of the IoT-based weighing system, including a detailed evaluation of data transmission reliability, latency, payload size, and server performance. These evaluations will ensure that the system is not only accurate and stable but also capable of delivering reliable weight data in real time. The combined findings will serve as the foundation for designing a robust IoT-based weight monitoring system suitable for industrial, commercial, and research purposes.

**Acknowledgments:** The authors would like to express their sincere gratitude to the academic community of the Faculty of Engineering, Universitas Muria Kudus, for their invaluable support throughout the course of this research. Particular recognition is given to the Informatics Engineering program for its valuable insights and collaboration, and to the Industrial Engineering Laboratory for its technical assistance in the fabrication and printing of the sensor-based models.

**Author contributions:** **Habiba, C., & Prayogo, A.:** Conceptualization, Methodology, Software, Validation, Investigation, Writing - original draft. **Habiba, C., & Prayogo, A.:** Methodology, Software, Formal analysis, Data curation. **Habiba, C., & Prayogo, A.:** Resources, Validation, Supervision. **Habiba, C., & Prayogo, A.:** Conceptualization, Methodology, Software, Supervision, Project administration, Writing - review & editing.

**Funding:** The study was conducted without any financial support from external sources.

**Availability of data and Materials:** All data are available from the authors.

**Conflicts of Interest:** The authors declare no conflict of interest.

**Additional Information:** No Additional Information from the authors.

## References

- [1] I. H. Khan and M. Javaid, "Role of Internet of Things (IoT) in Adoption of Industry 4.0," *J. Ind. Integr. Manag.*, vol. 7, no. 4, pp. 515–553, 2022.
- [2] T. Adame, A. Bel, A. Carreras, J. Melià-Seguí, M. Oliver, and R. Pous, "CUIDATS: An RFID–WSN hybrid monitoring system for smart health care environments," *Futur. Gener. Comput. Syst.*, vol. 78, no. 2, pp. 602–615, 2018, doi: <https://doi.org/10.1016/j.future.2016.12.023>.

- [3] D. B. Mariappan, H. Parihar, M. K. Gautham, and D. C. Verma, "Smart Office Area Monitoring & Control Based on IOT," 2020, doi: <https://doi.org/10.1109/ICACCCN51052.2020.9362896>.
- [4] B. Unhelkar, S. Joshi, M. Sharma, S. Prakash, A. K. Mani, and M. Prasad, "Enhancing supply chain performance using RFID technology and decision support systems in the industry 4.0—A systematic literature review," *Int. J. Inf. Manag. Data Insights*, vol. 2, no. 2, 2022, doi: <https://doi.org/10.1016/j.jjimei.2022.100084>.
- [5] A. Ustundag and M. Tanyas, "The impacts of radio frequency identification (RFID) technology on supply chain costs," *Transp. Res. Part E Logist. Transp. Rev.*, vol. 45, no. 1, pp. 29–38, 2009, doi: <https://doi.org/10.1016/j.tre.2008.09.001>.
- [6] A. Sarac, N. Absi, and S. Dauzère-Pérès, "A literature review on the impact of RFID technologies on supply chain management," *Int. J. Prod. Econ.* 128, vol. 128, no. 1, pp. 77–95, 2010, doi: <https://doi.org/10.1016/j.ijpe.2010.07.039>.
- [7] S. Erlangga, A. Yunita, and S. Satriana, "Development of Automatic Real-Time Inventory Monitoring System using RFID Technology in Warehouse," *Int. J. Informatics Vis.*, vol. 6, no. 3, 2022, doi: <https://dx.doi.org/10.30630/joiv.6.3.1231>.
- [8] J. U. M. Akbar, S. F. Kamarulzaman, A. J. M. Muzahid, M. A. Rahman, and M. Uddin, "A Comprehensive Review on Deep Learning Assisted Computer Vision Techniques for Smart Greenhouse Agriculture," *IEEE Access*, vol. 12, 2024, doi: <https://doi.org/10.1109/ACCESS.2024.3349418>.
- [9] W. Villegas-Ch, A. M. Navarro, and S. Sanchez-Viteri, "Optimization of inventory management through computer vision and machine learning technologies," *Intell. Syst. with Appl.*, vol. 24, 2024, doi: <https://doi.org/10.1016/j.iswa.2024.200438>.
- [10] M. A. Majdi, B. S. B. Dewantara, and M. M. Bachtár, "Product Stock Management Using Computer Vision," 2020, doi: <https://doi.org/10.1109/IES50839.2020.9231673>.
- [11] V. B. AYOOLA, G. OSAM-NUNOO, C. UMEAKU, BABATUNDE, and O. AWOTIWON, "IoT-driven Smart Warehouses with Computer Vision for Enhancing Inventory Accuracy and Reducing Discrepancies in Automated Systems," *IRE Journals*, vol. 8, no. 5, pp. 176–210, 2024.
- [12] A. Julian, A. A. A. K. B, and A. J. R, "Efficient Stock Management Using Computer Vision," 2024, doi: <https://doi.org/10.1109/CICN63059.2024.10847514>.
- [13] M.-H. Lin, M. A. Sarwar, Y.-A. Daraghmi, and T.-U. İk, "On-Shelf Load Cell Calibration for Positioning and Weighing Assisted by Activity Detection: Smart Store Scenario," *IEEE Sens. J.*, vol. 22, pp. 3455–3463, 2022, doi: <https://doi.org/10.1109/jsen.2022.3140356>.
- [14] H. A. Adam, M. Sari, W. S. A. Banjarnahor, O. B. Tumanggor, and D. F. Gultom, "Rice Stock Monitoring: A Smart-home Based System," *Int. J. Res. Vocat. Stud.*, vol. 2, no. 4, 2023, doi: <https://doi.org/10.53893/ijrvocas.v2i4.188>.
- [15] S. Budijono, J. Chrisnanda, R. O. Manorek, and I. Alexander, "Raw Material Inventory Monitoring System in The Food and Beverages," 2025, doi: <https://doi.org/10.1088/1755-1315/1488/1/012098>.
- [16] E. Žunić, S. Delalić, K. Hodžić, A. Beširević, and H. Hindija, "Smart Warehouse Management System Concept with Implementation," 2018, doi: <https://doi.org/10.1109/NEUREL.2018.8587004>.
- [17] G. Hemalatha, Akshay, L. Premkumar, Mukhunthan, and V. S. Raj, "INTELLIGENT INVENTORY MANAGEMENT SYSTEM," *Int. Res. J. Eng. Technol.*, vol. 11, no. 5, pp. 18–23, 2024.
- [18] M. N. Mansor, N. A. A. Talib, S. A. Saidi, W. A. Mustafa, and N. F. Zamri, "Arduino IoT-Based Inventory Management System Using Load Cell and NodeMCU," *J. Adv. Res. Appl. Sci. Eng. Technol.*, vol. 32, no. 3, 2023, doi: <https://doi.org/10.37934/araset.32.3.1225>.
- [19] S. Zhuang et al., "Temperature field analysis and compensation improvement of load cell," *Sci. Rep.*, vol. 14, 2024, doi: <https://doi.org/10.1038/s41598-024-76688-0>.
- [20] T. Saidi and A. El Bakkali, "Smart position detection of shelf-load based on imbalanced load cell sensors," in *IEEE International Conference on Advances in Data-Driven Analytics and Intelligent Systems (ADACIS)*, 2023, pp. 1–5, doi: <https://doi.org/10.1109/ADACIS59737.2023.10424158>.
- [21] F. Del Zozzo, G. Canavera, T. Frioni, E. Magnanini, and S. Poni, "A novel low-cost trunk load cell sensor for estimating canopy transpiration in the grapevine," *Agric. Water Manag.*, vol. 312, 2025, doi: <https://doi.org/10.1016/j.agwat.2025.109432>.
- [22] J. W. Simatupang and A. A. Ar-Rafif, "Prototype of A Smart Trash Bin for Trash Composting Based on Load Cell HX711 and Ultrasonic Sensors," *Serambi Eng.*, vol. 9, no. 1, pp. 8289–8301, 2024, doi: <https://doi.org/10.32672/jse.v9i1.1074>.
- [23] O. A. Leonov and N. Z. Shkaruba, "Investigation of the influence of load cell diameter on mass measurement error," 2024, doi: <https://doi.org/10.1063/5.0182257>.
- [24] S. Zhuang et al., "Analysis of Return-to-Zero Error after the First Load of Load Cell," *Sensors*, vol. 23, no. 21, 2023, doi: <https://doi.org/10.3390/s23218712>.
- [25] C. Zhou, M. Yuan, C. Feng, and W. T. Ang, "A Modified Prandtl–Ishlinskii Hysteresis Model for Modeling and Compensating Asymmetric Hysteresis of Piezo-Actuated Flexure-Based Systems," *Sensors*, vol. 22, no. 22, 2022, doi: <https://doi.org/10.3390/s22228763>.
- [26] Scaime, "Low cost single point load cell, 3 kg ... 5 kg," [scaime.com](https://scaime.com). <https://scaime.com/product/post/bef> (accessed Jun. 02, 2025).

- 
- [27] Valcom, "Single Point type Load Cell VPW6DC3 series," valcom.co.jp. <https://www.valcom.co.jp/english/product/lc/vpw6dc3/> (accessed May 28, 2025).
- [28] M. Intec, "MinebeaMitsumi Single Point Load Cell BCL-A," minebea-intec.com. <https://www.minebea-intec.com/us/load-cells/platform-scale-load-cells/single-point-load-cell-bcl-a> (accessed May 27, 2025).
- [29] Anyload, "108AA Single Point Load Cell," anyload.com. <https://www.anyload.com/product/108aa-single-point-load-cell/> (accessed May 27, 2025).
- [30] HBM (Hottinger Brüel & Kjær), "PW4M and PW4M-OP Single Point Load Cells for Precise Weighing of Masses from 300 g to 5 kg," hbm.com. [https://www.hbm.com/3026/pw4m-high-precision-miniature-load-cell/?product\\_type\\_no=PW4M+High-Precision+Miniature+Load+Cell+with+Certificate](https://www.hbm.com/3026/pw4m-high-precision-miniature-load-cell/?product_type_no=PW4M+High-Precision+Miniature+Load+Cell+with+Certificate) (accessed May 27, 2025).
- [31] Cardinal, "Cardinal LOAD CELLS Series TSP-Load Cells For Bench Applications." [Online]. Available: [https://www.controlsysteamsusa.com/controlsysteamsusa/download/Cardinal\\_TSP\\_LoadCells\\_Datasheet.pdf](https://www.controlsysteamsusa.com/controlsysteamsusa/download/Cardinal_TSP_LoadCells_Datasheet.pdf).